Numerical Investigation of Vibration Reduction Through IBC for a 20to Helicopter Rotor Model

D. Fürst
T. Auspitzer
ZF Luftfahrttechnik GmbH, Calden, Germany

M. T. Höfinger
B. G. van der Wall
Deutsches Zentrum für Luft- und Raumfahrt, Braunschweig, Germany

Abstract

This paper presents theoretical results of vibration reduction through IBC (Individual Blade Control) for a 20to helicopter rotor model which are based on numerical computations. The investigations were performed in order to analyse the efficiency of single and mixed mode IBC inputs on the helicopter vibrations of a model for a six bladed fully articulated rotor. Moreover, within this framework a method for the numerical investigations is proposed and validated. One important benefit of this method for the vibration reduction investigations is, that the computational effort can be decreased significantly. This reduction becomes possible, because a considerable portion of time consuming non linear computer simulations usually used for this purpose is replaced by numerical computations based on offline identified T-matrix models. It is shown, that the proposed method is well suited for vibration reduction investigations. Besides this, the potential of single and mixed mode IBC for reducing vibrations of the six bladed 20to rotor model will be presented in detail.

Notation

A_n	Amplitude of single mode n/rev IBC input, *deg*
c	Blade chord, *m*
C_T	Thrust coefficient, $C_T = 2T/(\rho\,(\Omega R)^2\,\pi R^2)$
J_{vib}	Vibration cost function
ΔJ_{vib}	Change of cost function due to IBC input, $\Delta J_{vib}=J_{vib,base}-J_{vib}$
$\mathbf{F}_x$	Vector of N/rev cosine and sine parts of non-rotating hub force in x-direction (propulsive force), *N*
$\mathbf{F}_y$	Vector of N/rev cosine and sine parts of non-rotating hub force in y-direction (side force), *N*
$\mathbf{M}_x$	Vector of N/rev cosine and sine parts of non-rotating hub roll moment, *Nm*
$\mathbf{M}_y$	Vector of N/rev cosine and sine parts of non-rotating hub pitch moment, *Nm*
n	Order of rotor harmonic component
N	Number of blades; number of measurement points
R	Rotor radius, *m*
R_A	Beginning of aerodynamic profile, *m*
R_E	Hinge offset, *m*
$\mathbf{T}$	Vector of N/rev cosine and sine parts of non-rotating hub force in z-direction (thrust), *N*
$\mathbf{T}_{1n}$	SIMO T-matrix, which maps n/rev IBC input to vibrations z_n, *N/deg, Nm/deg*
$\mathbf{T}_1$	MIMO T-matrix of linear T-matrix model, *N/deg, Nm/deg*
$\mathbf{T}_{2n}$	SIMO T-matrix of non-linear T-matrix model, which maps n/rev IBC input to vibrations z_n, *N/deg², Nm/deg²*
V	Forward speed, *m/s*
x_{cg}	Horizontal location of centre of gravity (c.g.), x_{cg}=0 for nominal location, *m*
$\mathbf{z}$	Vector of all N/rev vibration harmonics, decomposed in cosine and sine parts, *N,Nm*
$\mathbf{z}_n$	Vector of all N/rev vibration harmonics, resulting from a n/rev IBC input, *N,Nm*
z	Vector, representing N/rev cosine and sin portion of one force or moment (used in figures), *N, Nm*
$\|\Delta z\|$	$\|\Delta z\| = \|z_{base}\| - \|z\|$
z_{cg}	Vertical distance from the rotor hub centre to the centre of gravity; z_{cg} = 2.37, *m*
ϕ_n	IBC phase angle of single mode n/rev IBC input, *deg*
ϑ	blade pitch control angle, *deg*
$\boldsymbol{\vartheta}_n$	Vector of cosine and sine parts of n/rev single mode IBC input, *deg*
ϑ_{tw}	blade twist, *deg*
$\boldsymbol{\vartheta}_{IBC}$	Vector of cosine and sine parts of single or

Presented at the 28th European Rotorcraft Forum, 17 – 20 September 2002, Bristol.

	mixed mode IBC input, *deg*
$\vartheta_{IBC,opt}$	Vector of optimal cosine and sine parts of single or mixed mode IBC input, *deg*
β_0	Zero flapping (conus) angle, *deg*
Ω	Rotor rotational frequency, *rad/s*
ρ	Air density, kg/m^3
μ	Advance ratio, $\mu=V/(\Omega R)$
$\hat{(\,)}$	Estimation
$(\,)^T$	Transpose of x
$(\,)^{-1}$	Inverse
$(\,)_c$	Cosine part
$(\,)_s$	Sine part
$(\,)_{base}$	Baseline value (without IBC)
$(\,)_0$	
$\Delta(\,)$	Change of value due to IBC $\Delta(\,) = (\,)_{base} - (\,)$

1 Introduction and Motivation

The high potential of HHC (Higher Harmonic Control) and IBC to reduce helicopter vibration and noise emission has been demonstrated several times by wind tunnel tests, flight tests and theoretical investigations (cf. [2], [11], [14], [15], [16], [17], [18], [19], [20] and references within). Most of the wind tunnel and flight tests as most of the numerical investigations, too, were conducted with rotors for light weight helicopters. Hence, the experience concerning the potential of HHC/IBC to reduce helicopter vibrations for medium weight helicopters is relatively poor compared to the experience with light weight helicopters. To narrow this gap and ZFL's flight test campaign currently carried out with the medium transport helicopter CH-53G [17] motivated the investigations presented in this paper.
Within a co-operation of ZF Luftfahrttechnik GmbH (ZFL) and the German Aerospace Centre (DLR) it was therefore decided to undertake numerical investigations concerning the vibration reduction through IBC for a 20to helicopter rotor model.

2 Description of the Test Environment

In this section the test environment consisting of the implemented rotor model, the investigated flight conditions and the used simulation code is being described briefly.

2.1 Description of implemented rotor model

The knowledge of the forced blade deformation is relevant to simulate realistically the forces and moments of a helicopter rotor generated by a higher harmonic blade pitch variation. Transferred into the fixed frame these forces and moments represent the excitation of the fuselage motion. The resulting vibration level finally also depends on the modal shapes and frequencies of the helicopter fuselage.
To setup the rotor model the mode shapes of the main rotor blades and the corresponding frequencies were calculated using the Finite Element Method with an approach following *Houbolt/Brooks*, Ref. [1]. Thereafter, the mode shapes are represented by a polynomial of seventh order. The calculations in this paper were made with elastic blades, taking three flapping, two lead-lag and the first torsion mode into account.
The modelling of the rotor used for the investigation described in this paper is based on the main rotor data of the Sikorsky CH-53G helicopter. The six bladed rotor is fully articulated. The main characteristics of the rotor model are listed in Table 1.

Table 1: Basic data of the rotor model.

C_T	0.009
N	6
R	11*m*
C	0.72*m* (5% tapered tip)
R_E	0.61*m*
Ω	19.37*rad/s*
ϑ_{tw}	11°/R
$r(\vartheta_{tw}=0°)/R$	0.625
β_0	0.0*deg*
R_A	2.84*m* (r/R=0.26)

2.2 Description of investigated flight conditions

Trim calculations from hover up to an advance ratio of μ = 0.35 in level flight were carried out to set up a data base for a wide range of flight conditions. For all advance ratios the single parameters of an IBC input e.g. frequency, amplitude, and phase were varied in order to analyse the influence of these parameters on the higher harmonic rotor forces and moments, see Table 2. Mixed-mode IBC inputs in addition to the single mode 2-, 4-, 5-, 6- and 7/rev IBC harmonics were solely applied at two advance ratios μ = 0.15 and μ = 0.35. As motivated later in section 4.1, the detailed analysis and the validation of the proposed method of investigation concentrated on these two advance ratios. Furthermore, for all advance ratios reference data (baseline values without IBC) were generated. In addition the influence of centre of gravity variations on the baseline values were investigated.
The reference data were obtained by trimming the chosen rotor condition with respect to the corresponding rotor roll- and pitch moment, thrust and rotor shaft angle with the collective and cyclic controls. Since this was done with an assumed downwash geometry, the effect of the blade dynamics and aerodynamic loading distribution on the rotor wake geometry and vice versa was taken into account by iterative calculations until convergence was achieved.

Table 2: Matrix of investigated rotor conditions, level flight.

advance ratio μ	hover	0.05	0.1	0.15	0.2	0.225	0.25	0.275	0.3	0.35
c.g.-variation	X			X						X
IBC freq. variation		X	X	X	X		X		X	X
IBC phase variation	X	X	X	X	X	X	X	X	X	X
IBC amplitude variation	X	X	X	X	X		X		X	X
IBC mixed mode				X						X

The corresponding trim values of the rotor moments and forces were obtained by CAMRAD/JA [21] calculations. The calculation results for the vibration levels with IBC were obtained in the same way, now taking into account the influence of the higher harmonic blade pitch on the rotor wake and the blade dynamics.

2.3 Description of simulation code S4

The calculations were performed using DLR's rotor simulation code S4. The ability of S4 to calculate the effects of HHC or IBC for a given rotor condition and to compute high resolution airloads was used in several investigations of vibration reduction by HHC/IBC [2], for acoustic analysis [3], post-processing [4] as well as for dynamic stall investigation [5] and parametric rotor optimisation [6]. S4 has a modular structure with routines for aerodynamics, blade dynamics, different rotor wake models, rotor trim and the controls (conventional and HHC/IBC as well). The aerodynamic routine contains a non-linear semi-empirical mathematical model of the aerodynamic coefficients, which considers unsteady effects as well as compressibility, dynamic stall and radial flow [7], [8]. The rotor downwash was calculated with a prescribed wake geometry model following *Beddoe*s [9], modified by *van der Wall* [10]. It considers double vortex systems and the influence of higher harmonic control on the rotor wake.

3 The Method of Numerical Investigations

Within this contribution the numerical investigation of vibration reduction through IBC is proposed, used and validated. Both, the method and the corresponding computational steps are now described in detail.

The sequence of the separate computational steps are shown in Fig. 1. In step 0, the initialisation step, a wide data base (cf. Table 2, row one to four) is generated using the S4 code. Using the data set generated in step 0, in step 1 we perform the parameter identification process. To keep the following computational effort at a minimum a simple model is used firstly. In our case this means that a linear T-matrix model structure for the following identification process has to be chosen.

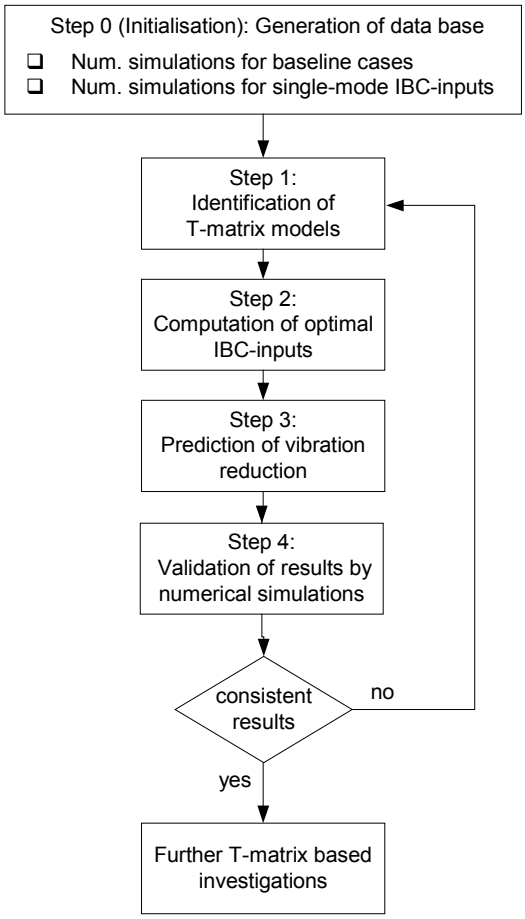

Fig. 1: Flow chart of the method used to investigate the vibration capabilities of IBC numerically.

This identification yields an identified T-matrix model, which maps the IBC inputs to the N/rev vibration components in the non-rotating frame, for single and for mixed mode IBC inputs as well. In step 2 an optimisation problem is solved considering the identified T-matrix model to compute the optimal (wrt. the vibration reduction task) single or mixed mode IBC inputs. Based on the computations performed before, predictions for the vibration reduction are computed in step 3. At the end of these steps the predictions are validated by further computer simulations with S4. If these simulation results were consistent with the predictions, further investigations could be carried out based on the identified linear T-matrix model. If not the described steps 1 to 4 needed to be repeated with a more complex T-matrix model structure, e.g. a non linear one. The introduction of an extended T-matrix model in the above described computational steps is motivated

by the fact that these models are able to improve the data fit. The improved data fit (respectively: the smaller identification errors) leads to more reliable computations in the subsequent steps of the overall method.
In the following subsections the computational steps are described in detail.

3.1 Generation of data base

The data base is generated using the rotor simulation code S4. A broad vibration data base of

- baseline (without IBC) and
- single mode IBC input

cases is generated (cf. Section 2). A single mode IBC input is defined as

$$\begin{aligned}\vartheta_n &= A_n \cdot \cos(n \cdot \Omega \cdot t - \phi_n) \\ &= \vartheta_{n,c} \cdot \cos(n \cdot \Omega \cdot t) + \vartheta_{n,s} \cdot \sin(n \cdot \Omega \cdot t) .\end{aligned}$$

This is the additional blade root pitch input due to IBC which is superposed on the conventional control input.

For each single mode IBC input computer simulations at least for one full IBC phase sweep (keep IBC amplitude A_n constant and vary the corresponding IBC phase angle ϕ_n in fixed increments) are conducted.
In the context of this paper, the vibrations are composed of the N/rev components of the rotor hub forces and moments in the non-rotating frame, decomposed in cosine and sine parts. The whole vector of vibrations $\mathbf{z}_n$ is defined as follows:

$$\mathbf{z}_n := \left[\mathbf{F}_x^T, \mathbf{T}^T, \mathbf{F}_y^T, \mathbf{M}_y^T, \mathbf{M}_x^T\right]_n^T \in \mathbb{R}^{10}$$

where

$$\mathbf{F}_x := [F_{x,c}, F_{x,s}]^T , \ \mathbf{F}_y := [F_{y,c}, F_{y,s}]^T , \ \mathbf{T} = [T_c, T_s]^T$$
$$\mathbf{M}_x := [M_{x,c}, M_{x,s}]^T , \ \mathbf{M}_y := [M_{y,c}, M_{y,s}]^T \in \mathbb{R}^2 .$$

The vibrations of the baseline cases are indicated with a zero as subscript, i.e. z_0. The single mode IBC-inputs ϑ_n is also represented by a vector of cosine and sine parts

$$\boldsymbol{\vartheta}_n := [\vartheta_{n,c}, \vartheta_{n,s}]^T \in \mathbb{R}^2 \ , n = 2,\ldots,p$$

where p represents the highest IBC input frequency.

3.2 Choice and identification of T-matrix models

Based on the vibration data generated in step 0, now the identification of the T-matrix model can be conducted. If the number of inputs is defined as the number of impressed IBC frequencies and the number of outputs as number of regarded forces and moments, for each IBC input ϑ_n a SIMO T-matrix model is identified.
In this paper two different T-matrix models are used, one of linear and one of non-linear type [11], to build up the above described mapping. These two models are introduced subsequently.

Linear SIMO T-matrix Models:

$$\hat{\mathbf{z}}_n = \hat{\mathbf{T}}_{1n} \cdot \boldsymbol{\vartheta}_n + \hat{\mathbf{z}}_{0n} \ , n = 2,\ldots,p \ , \ \hat{\mathbf{T}}_{1n} \in \mathbb{R}^{10,2} \ .$$

Non-linear SIMO T-matrix Models:

$$\hat{\mathbf{z}}_n = \hat{\mathbf{T}}_{1n} \cdot \boldsymbol{\vartheta}_n + \mathrm{diag}\{\mathrm{diag}\{\boldsymbol{\vartheta}_n\}\} \cdot \hat{\mathbf{T}}_{2n} \cdot \boldsymbol{\vartheta}_n + \hat{\mathbf{z}}_{0n} ,$$
$$n = 2,\ldots,p \ ; \ \hat{\mathbf{T}}_{1n}, \hat{\mathbf{T}}_{2n} \in \mathbb{R}^{10,2} .$$

For both model structures the parameter identification of $\hat{\mathbf{T}}_{1n}$, $\hat{\mathbf{z}}_{0n}$ an $\hat{\mathbf{T}}_{2n}$ (if required) is based on the least squares method, i.e. the error

$$\boldsymbol{\varepsilon}_z^2 = \frac{1}{2}(\boldsymbol{\varepsilon}_z^T \cdot \boldsymbol{\varepsilon}_z) = \frac{1}{2}(\mathbf{z} - \hat{\mathbf{z}})^T \cdot (\mathbf{z} - \hat{\mathbf{z}})$$

is minimised. For the linear T-matrix models the identification equations are described subsequently. Let N be the number of data points for the IBC input $\boldsymbol{\vartheta}_n$. We define:

$$\underbrace{[\mathbf{z}_{n1}, \ldots \mathbf{z}_{nN}]}_{=:\mathbf{Z}_n} = \hat{\mathbf{T}}_{1n}^* \cdot \underbrace{[\boldsymbol{\vartheta}_{n1}^*, \ldots, \boldsymbol{\vartheta}_{nN}^*]}_{=:\boldsymbol{\Theta}_n}$$

where

$$\boldsymbol{\vartheta}_{ni}^* := \left[\boldsymbol{\vartheta}_{ni}^T, 1\right]^T \in \mathbb{R}^3$$

and

$$\hat{\mathbf{T}}_{1n}^* := [\hat{\mathbf{T}}_{1n}, \hat{\mathbf{z}}_{on}] \in \mathbb{R}^{10,3} .$$

Then the estimation of the T-matrix parameters and the baseline vibration level is computed by

$$\hat{\mathbf{T}}_{1n}^* = \mathbf{Z}_n \cdot \boldsymbol{\Theta}_n^T \cdot \left[\boldsymbol{\Theta}_n \cdot \boldsymbol{\Theta}_n^T\right]^{-1} .$$

For a detailed description of the identification equations of the non-linear T-matrix model the reader is referred to [11] .
The above SIMO T-matrix models describe the transfer behaviour from a single mode IBC input $\boldsymbol{\vartheta}_n$ to all regarded vibration components $\mathbf{z}_n$. In order to investigate the impact of single and mixed mode IBC inputs on the helicopter vibrations we assemble the identified SIMO T-matrix models to an overall MIMO T-matrix model. This model maps all IBC inputs to all vibration components. The assembly leads to a linear MIMO T-matrix model of type

$$\hat{\mathbf{z}} = \underbrace{\left[\hat{\mathbf{T}}_{12}, \ldots, \hat{\mathbf{T}}_{1p}\right]}_{=:\hat{\mathbf{T}}_1} \cdot \underbrace{\begin{bmatrix} \boldsymbol{\vartheta}_2 \\ \vdots \\ \boldsymbol{\vartheta}_p \end{bmatrix}}_{=:\boldsymbol{\vartheta}_{IBC}} + \hat{\mathbf{z}}_0 .$$

In the case of the non-linear model type we obtain

$$\hat{\mathbf{z}} = \underbrace{\left[\hat{\mathbf{T}}_{12}, \ldots, \hat{\mathbf{T}}_{1p}\right]}_{=:\hat{\mathbf{T}}_1} \cdot \underbrace{\begin{bmatrix} \boldsymbol{\vartheta}_2 \\ \vdots \\ \boldsymbol{\vartheta}_p \end{bmatrix}}_{=:\boldsymbol{\vartheta}_{IBC}} + \sum_{n=2}^{p} \mathrm{diag}\{\mathrm{diag}\{\boldsymbol{\vartheta}_n\}\} \cdot \hat{\mathbf{T}}_{2n} \cdot \boldsymbol{\vartheta}_n + \hat{\mathbf{z}}_0 .$$

In both cases the identified baseline vibrations of the MIMO models are given by:

$$\hat{\mathbf{z}}_0 = \frac{1}{p-1}\sum_{n=2}^{p}\hat{\mathbf{z}}_{0n} \ .$$

Finally, for every investigated flight condition the transfer behaviour from all regarded IBC inputs to the vibrations is described by an identified MIMO T-matrix model of above type.

Remark (non-linear T-matrix model): In [11] it was shown, that compared to the linear T-matrix model the non-linear T-matrix model is better suited to represent the transfer behaviour from 2/rev IBC inputs to measured 4/rev fuselage vibrations of a four bladed helicopter. Therefore, these non-linear models play an important role, if the impact of 2/rev IBC is investigated. In this paper we will see, that the non-linear T-matrix model is also better suited to represent the transfer behaviour from other than 2/rev IBC inputs to N/rev vibrations as linear T-matrix models and therefore lead to more reliable computations.

3.3 Optimal single and mixed mode IBC inputs

Based on the identified MIMO T-matrix model the optimal (regarding the vibration reduction task) single or mixed mode IBC inputs (step 3) are computed. In general, these inputs are computed by solving the following optimisation problem: For the given identified linear or non-linear MIMO T-matrix model select ϑ_{IBC} such that the cost function

$$J_{vib} = \sqrt{\frac{\mathbf{F}_x^T\mathbf{F}_x}{w_1^2} + \frac{\mathbf{T}^T\mathbf{T}}{w_2^2} + \frac{\mathbf{F}_y^T\mathbf{F}_y}{w_3^2} + \frac{\mathbf{M}_y^T\mathbf{M}_y}{w_4^2} + \frac{\mathbf{M}_x^T\mathbf{M}_x}{w_5^2}}$$

will be minimised. For the computations in this paper we chose the weighting factors as $w_1 = w_2 = w_3 = 1$ and $w_4 = w_5 = z_{cg}$. With this choice of w_4 and w_5 the associated moments are transformed into equivalent forces at the centre of gravity. This physical motivated weighting is performed, in order to prevent an overrating of the moments compared to the forces in the above cost function.
In case of a linear T-matrix model the solution of the optimisation problem leads to

$$\vartheta_{IBC,opt} = \left[\hat{\mathbf{T}}_1^T \cdot \overline{\mathbf{W}} \cdot \mathbf{T}_1\right]^{-1} \cdot \hat{\mathbf{T}}_1^T \cdot \overline{\mathbf{W}} \cdot \hat{\mathbf{z}}_0$$

where $\mathbf{W}$:=diag(w_1, w_1,..., w_5,w_5), $\overline{\mathbf{W}} := \mathbf{W}^T \cdot \mathbf{W}$. When the non-linear T-matrix model is used the solution of the optimisation problem can not be solved analytically in the above manner. Instead, the solution has to be computed with numerical search algorithms. For the investigations in this paper a numerical implementation based on a simulated Annealing Algorithm is used. This choice is based on the property, that the Annealing Algorithm is a global optimisation method. In order to enable the detection of the global minimum, the algorithm allows uphill steps and thus it can escape from local minima. This is not true for gradient based search algorithms. The implemented algorithm is based on a Fortran subroutine described in [12],[13].

3.4 Achievable vibration reduction

With the identified MIMO T-matrix models and the calculated optimal IBC inputs predictions of the achievable vibration reduction can be calculated by

$$\Delta J_{vib}[\%] = \frac{J_{vib}(\vartheta = 0) - J(\vartheta_{opt})}{J_{vib}(\vartheta = 0)} \cdot 100 \ .$$

To perform this calculation the vibrations $\hat{\mathbf{z}}$, which result if the optimal IBC inputs $\vartheta_{IBC,opt}$ are applied, are predicted with the corresponding identified MIMO T-matrix models. E.g., for the linear T-matrix model this is done by

$$\mathbf{z} = \hat{\mathbf{T}}_1 \cdot \vartheta_{IBC,opt} + \hat{\mathbf{z}}_0 \ .$$

3.5 Validation of the predicted results

To validate the T-matrix based results calculated in the previous steps, in particular the predicted vibration reductions, S4 simulations with optimised IBC inputs $\vartheta_{IBC,opt}$ are performed. The predicted vibration reductions and the calculated vibrations obtained with S4 are compared. By judging the consistency of both results, it has to be decided, whether the repeat of steps 1 to 4 with a more complex T-matrix model might be necessary to improve the reliability of the T-matrix based calculations.

4 Numerical Results using linear T-Matrix Models

In this section the numerical results of step 0 (cf. Fig. 1) and the results obtained using a linear T-matrix models are presented and discussed.

4.1 Baseline cases and single mode IBC phase sweeps

Here the results of step 0 are presented. This includes the data base generation for the baseline cases without IBC and the cases with single mode IBC using the rotor simulation code S4. Because of the large amount of generated data only a representative fraction of this data can be presented here. The baseline vibrations of the implemented rotor model rise from low levels in hover to a maximum at an advance ratio of about 0.1 in level flight, Fig. 2.

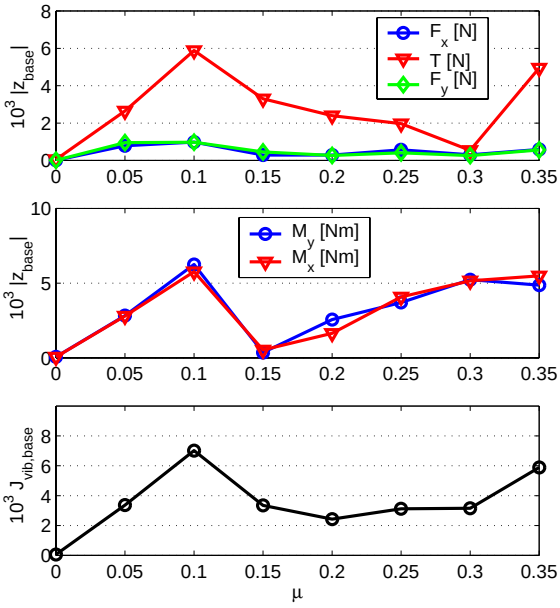

Fig. 2: Calculated baseline vibration amplitudes and cost function J_{vib} vs. μ, level flight (S4 results).

With higher forward speeds, the vibration level decreases, before rising again to higher levels in high speed forward flight. At $\mu = 0.15$ the N-harmonic rotor moments in the fixed frame reach a local minimum. A reduction of the overall vibration level J_{vib} at this rotor condition therefore is equivalent to reducing the thrust alone without increasing the other forces and moments. At $\mu = 0.35$ both, thrust and rotor moments, reach high levels. Because of this our analysis focused on these two different rotor conditions.

Results of simulation calculations with different centre of gravity (c.g.) offsets but constant helicopter Take Off Weight showed, that the location of the centre of gravity has a negligible influence on the N-harmonic rotor forces and moments and therefore on the vibration level, Fig. 3. Hence c.g. variations are not considered in further investigations.

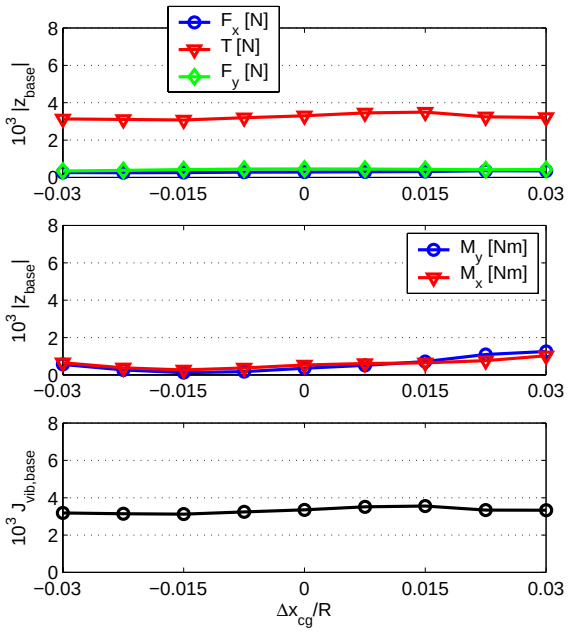

Fig. 3: Calculated baseline vibration amplitudes and cost function J_{vib} vs. c.g. location, level flight, $\mu = 0.15$, $C_T = 0.00901$ (S4 results).

In Fig. 4 to Fig. 7 the calculated changes of the vibration amplitudes and the resulting cost-function J_{vib} due to 4/rev and 6/rev IBC for μ=0.15 and μ=0.35 are shown.

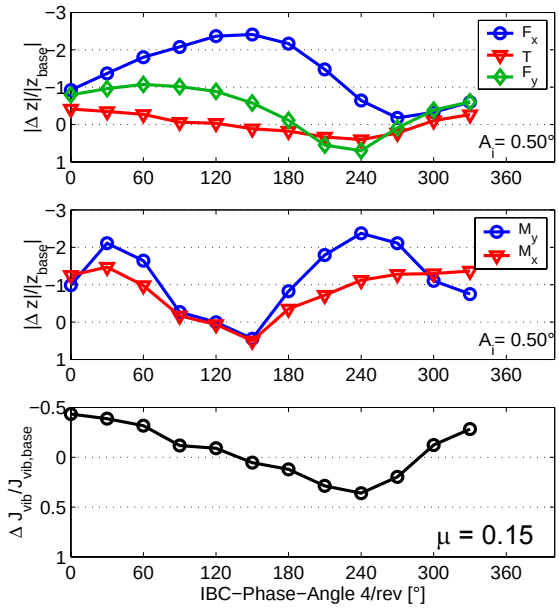

Fig. 4: Calculated changes of vibration amplitudes and of cost function J_{vib} due to 4/rev IBC with A_4=0.5° at μ=0.15 (S4-results).

In Fig. 4 it can be seen, that 4/rev IBC has a considerable influence on the vibration level at μ=0.15. For the IBC Amplitude A_4=0.5° an overall vibration reduction of about 40 percent is achieved at ϕ_4=240°. Furthermore it can be seen that this reduction is caused by the reduction of T and F_y only. All other

vibration levels are increased at this IBC phase angle and amplitude.

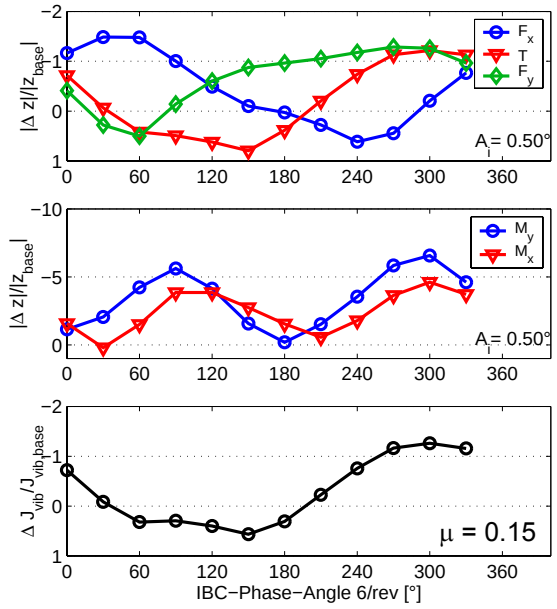

Fig. 5: Calculated changes of vibration amplitudes and of cost function J_{vib} due to 6/rev IBC with A_6=0.5° at μ=0.15 (S4-results).

The same situation can be seen in Fig. 5 for 6/rev IBC. At ϕ_6 = 150° an overall vibration reduction of about 50 percent is achieved by a reduction of T alone, whereby all other forces and moments are increased. In particular for 6/rev IBC, the moments are increased up to seven hundred percent for almost every IBC phase angle. This indicates that the applied IBC amplitude A_6=0.5° is too high for a reduction of the moments.

The above facts can be summarised as follows: The IBC amplitude and IBC phase angle requirements for a vibration reduction of each component with 4/rev or 6/rev IBC are different and therefore a simultaneously reduction of all components is not possible. This can also be seen partly in Fig. 6 and Fig. 7 for 4/rev and 6/rev IBC at μ = 0.35.

Furthermore this observation is valid for almost all cases of the remaining IBC frequencies 2,5 and 7/rev. These first results concerning the vibration reduction capabilities of single mode IBC indicates that for a considerable vibration reduction of the investigated 20to rotor model mixed mode IBC plays an important role or even seems to be necessary.

This numerical result coincides quite fine with first flight test results of an IBC system for the CH-53G helicopter, presented in [17]. The examination of the flight test data in [17] showed that in several cases the optimal IBC amplitudes and phase angles for different sensor orientations do not coincide. Therefore single mode IBC becomes less effective if it is required to reduce vibrations at different locations and in all axes simultaneously.

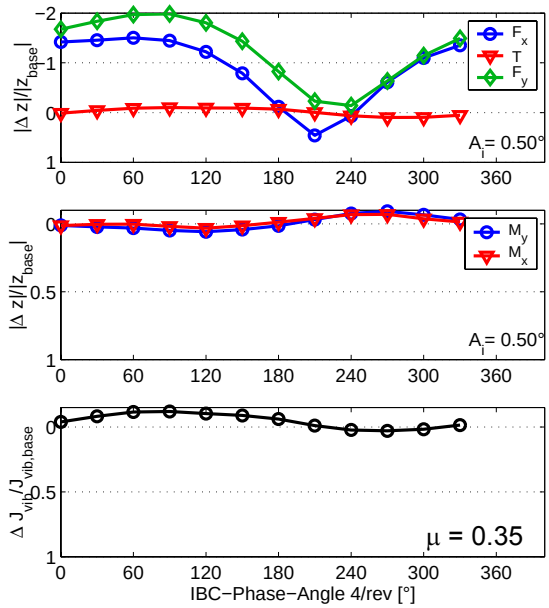

Fig. 6: Calculated changes of vibration amplitudes and of cost function J_{vib} due to 4/rev IBC with A_4=0.5° at μ=0.35 (S4-results).

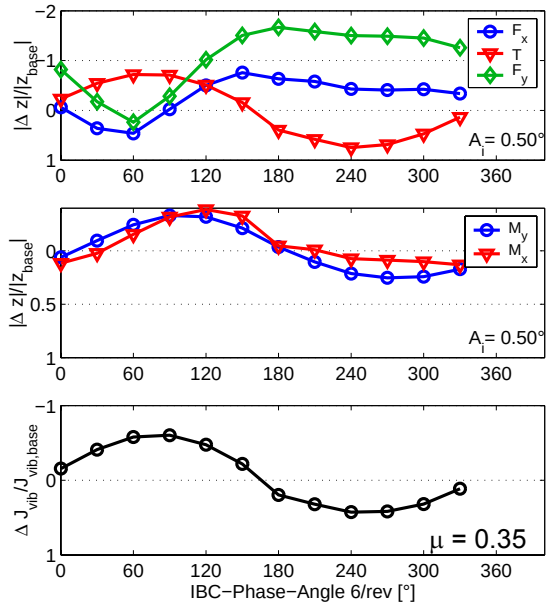

Fig. 7: Calculated changes of vibration amplitudes and of cost function J_{vib} due to 6/rev IBC with A_6=0.5° at μ=0.35 (S4-results).

The above motivated requirement for mixed mode IBC complicates the vibration reduction task and the corresponding numerical investigations. Therefore the need for a systematic and effective investigation method is emphasised by the above results. This is a further motivation for the validation of the method proposed in this paper.

4.2 Identification and optimisation results

Based on the generated data base the identification of T-matrix models and the computation of optimal single and mixed mode IBC inputs were performed.

In Fig. 8 to Fig. 11 the identified linear SIMO T-matrix models for 4/rev and 6/rev IBC are shown exemplaryly. The IBC affected vibrations computed with S4 are marked by the small circles. The added solid curve in each figure represents the T-matrix based estimations. The estimated values and the values, computed by S4, are connected by short lines. Each line represent the identification error of the corresponding data point.

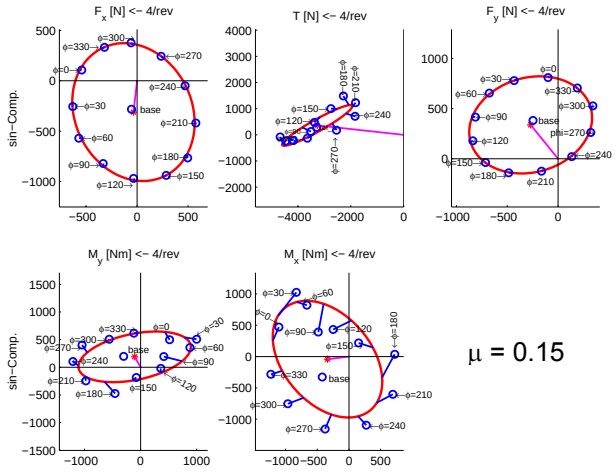

μ = 0.15

Fig. 8: Identified linear SIMO T-matrix model for 4/rev IBC at μ=0.15.

From this graphical representation it is possible to decide uniquely whether the A_i used has been chosen to large or to small. In Fig. 8 we see that the applied IBC amplitude $A_4 = 0.5°$ is to large for a vibration reduction of F_x, M_x and M_y. Furthermore, it is indicated that the impact on T is small.

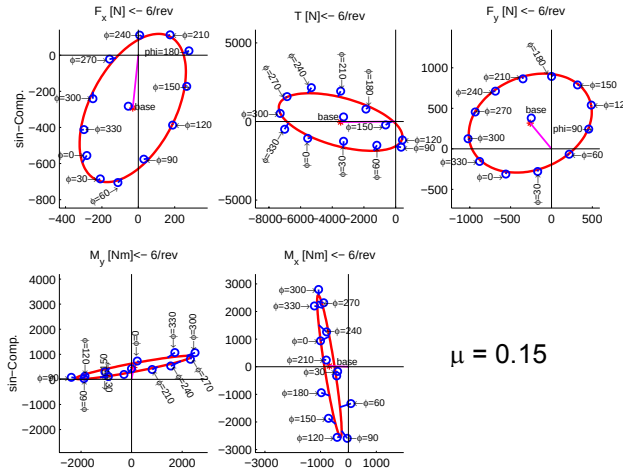

μ = 0.15

Fig. 9: Identified linear SIMO T-matrix model for 6/rev IBC at μ=0.15.

In Fig. 9 it is indicated that 6/rev have a good effectiveness on F_x, F_y and T, but different IBC phase angles are required for the vibration reduction. At μ = 0.35 4/rev IBC has a good impact on F_x and F_y, but only a small impact on the moments and on thrust (cf. Fig. 10).

From the above results the following general conclusions can be drawn:

- Most data points can be represented quite fine by linear SIMO T-matrix models. The identification errors for higher advance ratios and HHC frequencies are smaller compared to the rest.
- 4/rev inputs have a considerable impact on the vibrations and can therefore be a valuable supplement in mixed mode IBC.
- For a simultaneous reduction of all vibration components different single mode IBC inputs are necessary and therefore IBC mixed mode will be needed.
- In some cases the applied IBC amplitudes are too large to reduce single vibration components.

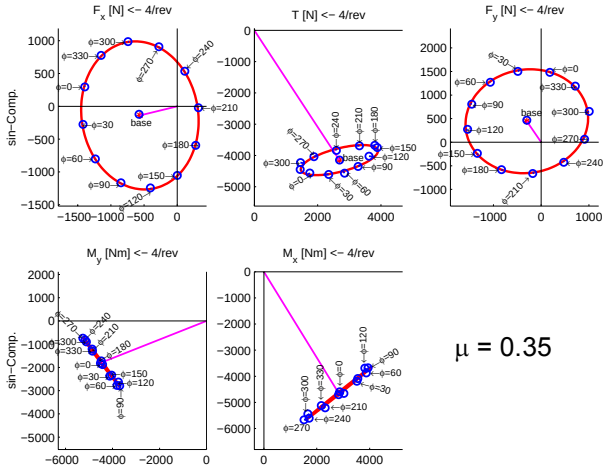

μ = 0.35

Fig. 10: Identified linear SIMO T-matrix model for 4/rev IBC at μ=0.35.

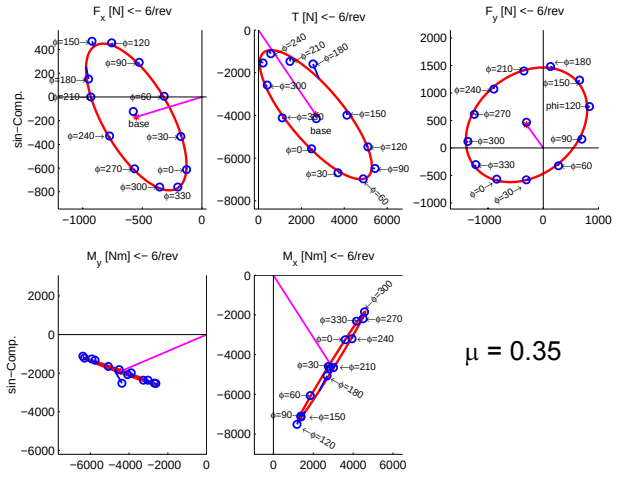

μ = 0.35

Fig. 11: Identified linear SIMO T-matrix model for 6/rev IBC at μ=0.35.

With the identified T-matrix models the optimisation problem as defined in Section 3.3 was solved for every possible combination of 4,5,6 and 7/rev IBC input. In Table 3 eleven different IBC harmonic combinations are listed exemplaryly.

Table 3: IBC cases

case	IBC frequency [n/rev]
1	4
2	5
3	6
4	7
5	4+6
6	5+6
7	5+7
8	4+5+6
9	4+6+7
10	5+6+7
11	4+5+6+7

The 2/rev is neglected in the following vibration reduction investigation because of the relative small impact on the vibrations of the six bladed rotor. However, the IBC frequency 2/rev seems to be more suited for BVI (noise) reduction purposes. The calculated optimal amplitudes of different single and mixed mode IBC cases at $\mu = 0.15$ and $\mu = 0.35$ as listed in Table 3 are given in Fig. 12.

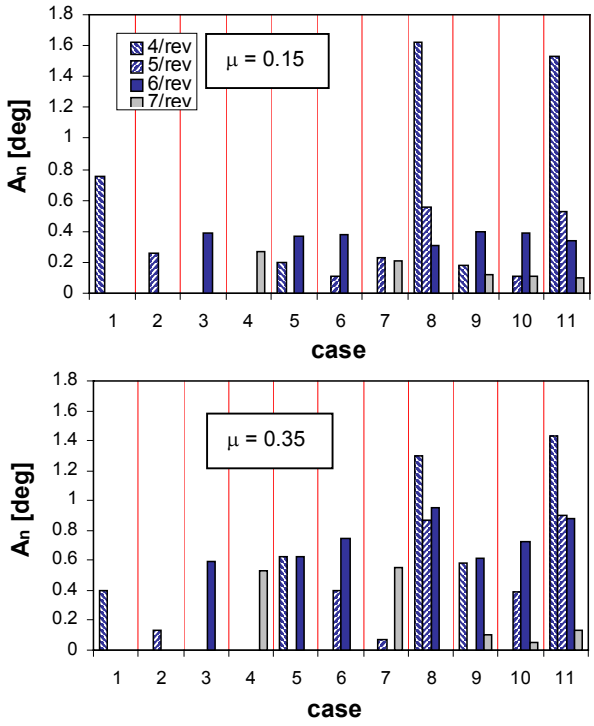

Fig. 12: Calculated optimal IBC amplitudes A_n (based on identified linear T-matrix model) for different IBC cases.

Except for the 4/rev amplitude of cases 8 and 11 the optimal IBC amplitudes for the given cases are below 1.0deg. Generally, they are greater at the higher advance ratio. The 7/rev amplitude is very small when used in mixed mode IBC in combination with more than two other harmonics, see cases 9, 10 and 11 in Fig. 12.

4.3 Predicted vibration reduction, validation and problem description

After determination of the optimal IBC inputs for maximum vibration reduction (concerning the minimisation of J_{vib}) with the linear T-matrix model, S4 calculations were performed with these optimised IBC inputs in order to validate the predicted vibration reductions.

It can be seen in Fig. 13 that the vibration reduction predictions based on the identified linear T-matrix models (indicated as linear T-matrix in Fig. 13) coincide in almost all cases very good with the vibrations computed by S4 (indicated as S4 in Fig. 13). This result indicates that already the linear T-Matrix model represents a pretty good mapping of the transfer behaviour of IBC inputs to the vibrations, especially for the advance ratio $\mu = 0.35$. But as indicated in Fig. 13 there are some cases where the identification based calculations led to bad predictions, especially if the two harmonics 4/rev and 5/rev were combined in mixed mode IBC at $\mu = 0.15$, see case 8 and 11 in Fig. 13.

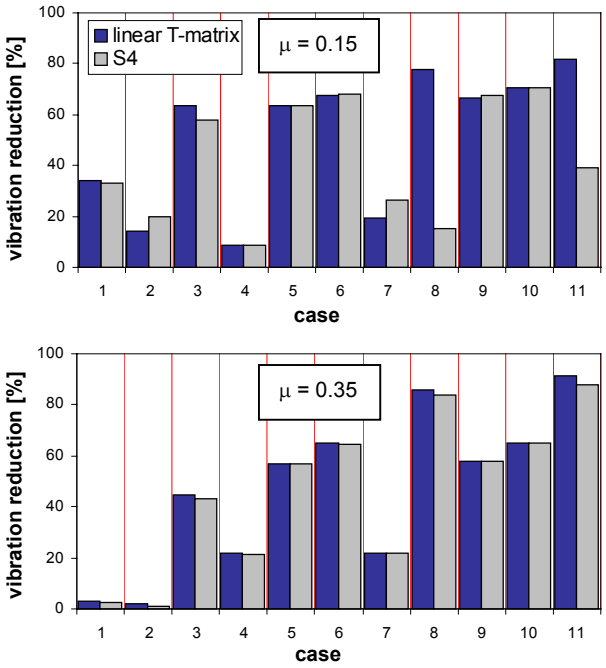

Fig. 13: Comparison of vibration reductions, predicted by linear T-matrix-model and vibration reductions, computed by S4.

In Fig. 14 the identification errors ε_z of all identified linear T-matrix models are shown. These errors are represented in percent, i.e.

$$\varepsilon_z[\%] := \frac{|z - \hat{z}|}{|z|} \cdot 100 \,.$$

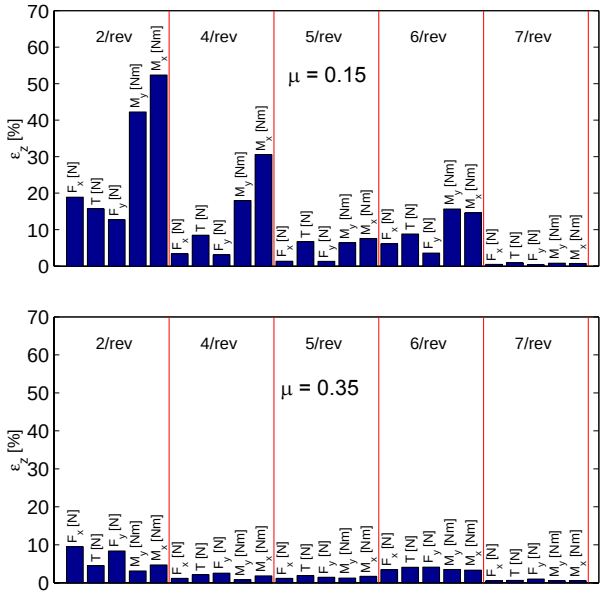

Fig. 14: Identification errors of the identified linear SIMO T-matrix models.

In Fig. 14 it can be seen that the identification errors for $\mu = 0.35$ are much smaller than for the lower advance ratio $\mu = 0.15$, in particular for non HHC frequencies. This substantiates the fact that the vibration predictions for $\mu = 0.35$ in Fig. 13 coincide very well with the vibration reductions computed by S4. Furthermore, Fig. 14 indicates that at $\mu = 0.15$ the identification errors, especially for the mappings of 4/rev IBC to M_x and M_y, are large compared to the rest.

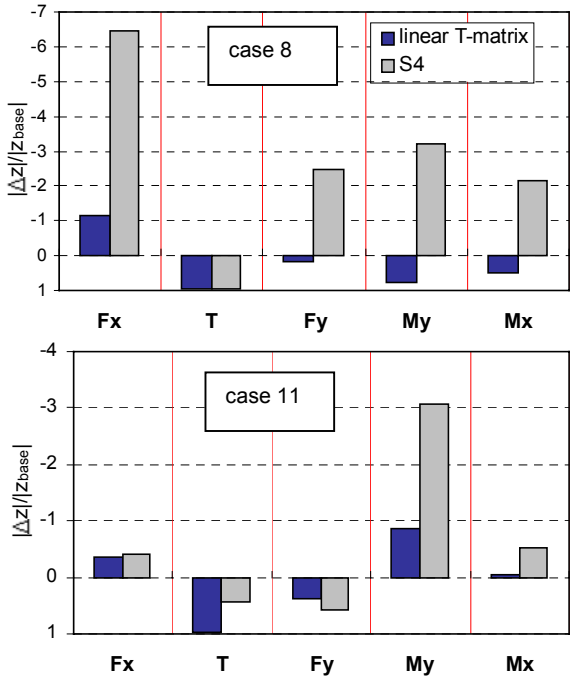

Fig. 15: Comparison of vibration reductions, predicted by linear T-matrix model and vibration reductions, computed by S4, level flight, $\mu = 0.15$, $C_T = 0.00901$.

Clearly, these identification errors could be the reason for the sub-optimal IBC inputs and the bad predictions, as presented for J_{vib} in Fig. 13 and for the single components of **z** in Fig. 15.

To solve this problem it was necessary to improve the data fit of the T-matrix model in these cases and thus to improve the reliability of the subsequent calculations.
This was done by repeating step 1 to 4 of the overall method, now with the non-linear MIMO T-matrix models, as introduced in Section 3. In Section 5 it is shown that this model is capable of reducing the identification errors. This leads to consistent results concerning the predicted vibration reduction in the critical cases.

5 Numerical results using improved T-matrix models

In this section the numerical results of the second step of the overall method are presented. The following presentation will focus on the two critical cases.

5.1 Identification and optimisation results

In Fig. 16 the identified non-linear SIMO T-matrix model for 4/rev IBC at $\mu = 0.15$ is shown exemplary.

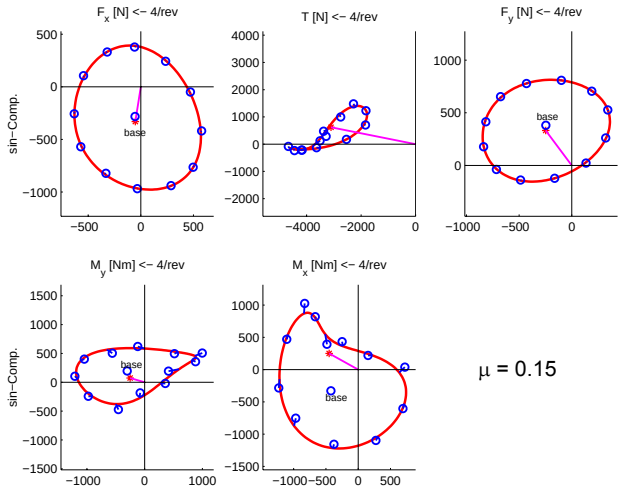

Fig. 16: Identified linear SIMO T-matrix models for 4/rev IBC at $\mu = 0.15$.

It can be stated that the non-linear model leads to a better data fit than the linear one (cf. Fig. 8). Moreover, the non-linear part of the model can be recognised in the curves of the identified vibrations. They do not show the classical ellipse shape, as known from the linear T-matrix models. In Fig. 17 the corresponding identifications errors for all SIMO T-matrix models are illustrated.

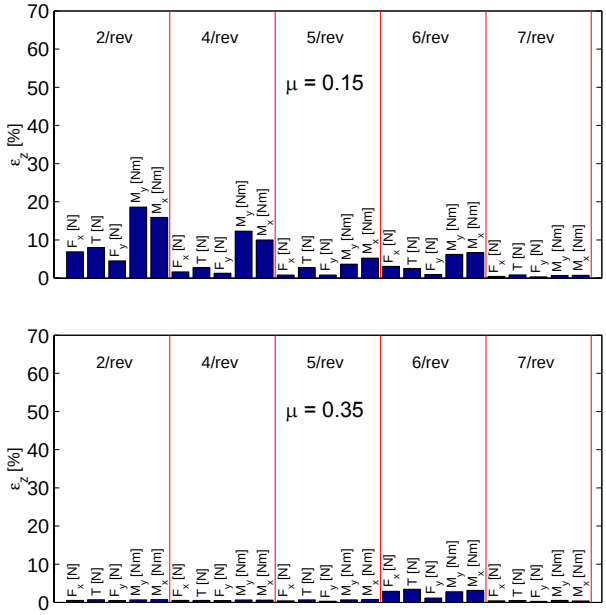

Fig. 17: Identification errors of the identified non-linear SIMO T-matrix models.

The above figures verify the better data fit of the non-linear T-matrix models. For example, the identification error for the mapping of 4/rev IBC to M_x could be decreased from 30 percent to 10 percent.
The optimal IBC inputs, (calculated) based on the non-linear T-matrix model and the predicted vibration reductions now coincide much better with the S4 results. The optimal IBC inputs differ to those determined with the linear T-matrix model, see Fig. 18.

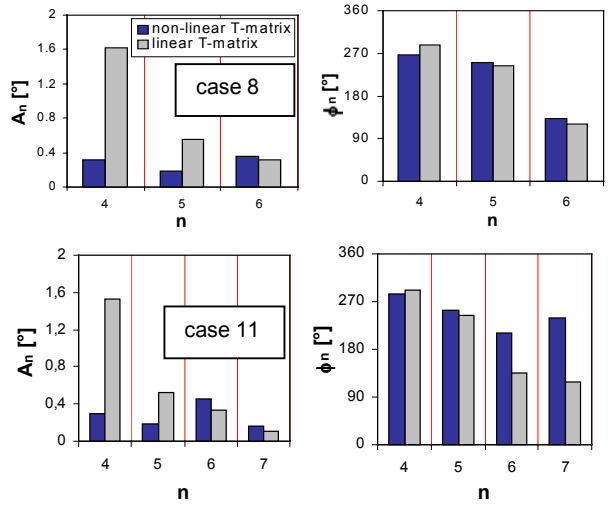

Fig. 18: Comparison of optimal IBC inputs, calculated based on linear and non-linear T-matrix models, level flight, $\mu = 0.15$, $C_T = 0.00901$.

5.2 Vibration reduction and validation

The predicted vibration reduction, now determined by the non-linear T-matrix model, was again validated with S4. A better prediction of the components of the vibration vector **z** for the presented cases 8 and 11 is achieved, compare Fig. 19 to Fig. 15. As a result, the vibration reduction, represented by the cost function J_{vib} shows very good agreement, compare Fig. 20 to Fig. 13.

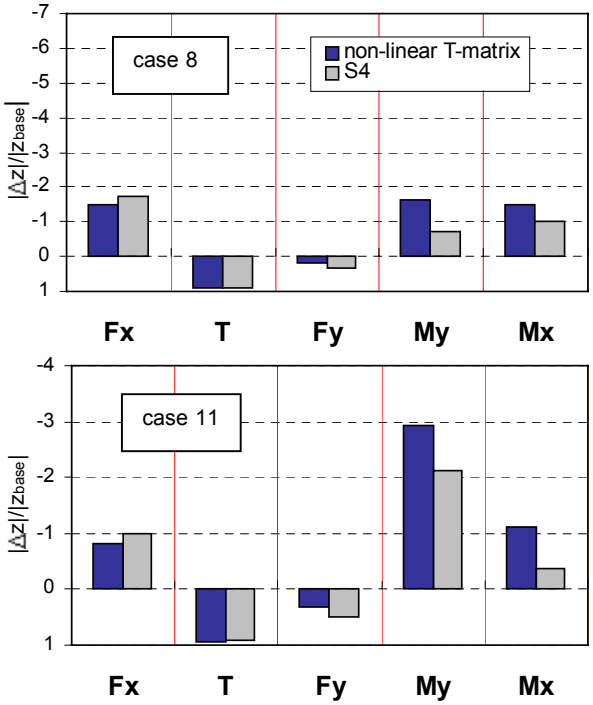

Fig. 19: Comparison of vibration reductions, predicted by non-linear T-matrix model and vibration reductions, computed by S4, level flight, $\mu = 0.15$, $C_T = 0.00901$.

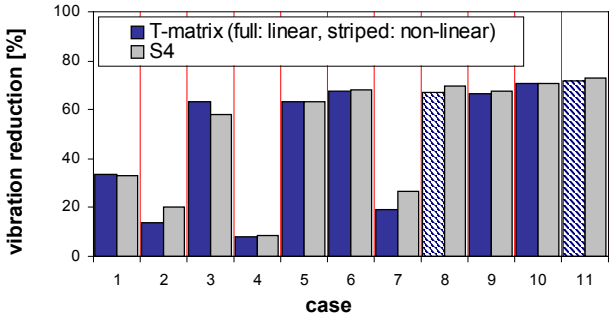

Fig. 20: Comparison of vibration reductions predicted by non-linear T-matrix model and vibration reductions computed by S4 for different IBC cases, level flight, $\mu = 0.15$, $C_T = 0.00901$.

Thus, from the investigation the following result can be stated: When non-linear T-matrix models are used to represent the mapping of the IBC-inputs to the vibrations in the critical cases, the vibration predictions coincide very good with the values computed by S4. This result shows that it is favourable to use a non-linear T-matrix model for the modelling of IBC induced vibrations, in particular for low speed cases and non HHC frequencies. It should be noted here that besides these two critical cases all remaining results based on the identified non-linear T-matrix model coincide good with the results obtained with the linear T-matrix model. These promising results encourage us to perform the further vibration

reduction investigations of this paper only based on the identified non-linear T-matrix model without further S4 simulations for validation purposes. A selection of these results is presented in the following subsection.

5.3 Further Results

Here, the achievable vibration reductions over the entire range of advance ratio were predicted using the identified non-linear T-matrix models. A graphical summary of these results is presented in Fig. 21.

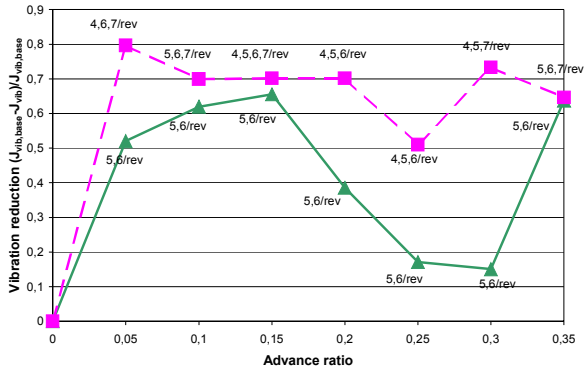

Fig. 21: Predicted achievable vibration reduction with different IBC mixed mode inputs vs. advance ratio.

The predicted achievable vibration reductions with 5+6/rev mixed mode IBC is represented by the solid line with triangle markers. This mixed mode is chosen, because it seems to offer a good compromise between the vibration reduction over a wide range of μ and the number of required frequencies. It should be noticed here that 5+6/rev IBC does not lead to the highest vibration reduction at any advance ratio. The best combination of two IBC-frequencies strongly depends on the advance ratio. Furthermore the optimal IBC amplitudes and phase angles also depend on the advance ratio (not shown here).
The dashed line in Fig. 21 with square markers represents the predicted vibration reductions with the best mixed mode combination. It can be seen that the 5+6/rev combination is less effective to reduce the vibration at $\mu = 0.2$ to $\mu = 0.3$. Especially for these advance ratios, combinations with 4/rev lead to a better vibration reduction. Moreover, it is indicated, that combinations of the IBC frequencies 4,5,6 and 7/rev lead to a considerable vibration reduction between 50 to 80% .

6 Results

Following the proposed method with a linear T-matrix approach at first, a good compliance of the predicted vibration reductions for the also calculated optimal IBC inputs with the results of the calculations with S4 was already achieved for several single and mixed mode IBC control inputs and flight conditions. However, for some mixed mode inputs and flight conditions a big difference between the prediction based on the T-matrix approach and the result of the calculations with S4 was observed.
By extending the linear T-matrix formalism with a non-linear term the match between the predicted vibration reductions and the reductions resulting from S4 was improved significantly. For the given rotor model the system behaviour is much better described with the non-linear T-matrix approach than with the linear T-matrix. Therefore the non-linear T-matrix model is better suited for T-matrix based investigations of vibration reduction. It is not limited to 2/rev IBC investigations.

As expected from the theory and prior studies our calculations underline once again the high efficiency of IBC to reduce vibrations. This holds also true for the chosen rotor model despite the different properties in comparison with e.g. Bo105 rotor.
In detail, the results in this paper obtained from our numerical simulations lead to the following findings regarding the vibration reduction possibilities and the associated IBC inputs:

1. For a considerable vibration reduction between 50 to 80 percent over the entire range of the advance ratio mixed mode IBC is necessary.
2. The frequencies and their number for the optimal mixed mode IBC input vary depending on the flight conditions.
3. The optimal IBC input for some flight conditions requires a 4/rev component which is a non HHC frequency. That means this kind of input can only be generated by an IBC system with actuators in the rotating frame.

Furthermore it was shown, that the proposed T-matrix based method is well suited for the investigation of the vibration reduction possibilities with IBC. To increase the reliability of the results it is favourable to use a non-linear T-Matrix model instead of classical linear one in the overall method.
However, it must be stated that these conclusions have been drawn from numerical simulations solely. The findings of our investigation and the feasibility of the proposed method still need to be verified on hand of data from the on going flight trials with the CH-53G.

7 Conclusion and Outlook

In this paper results of numerical calculations for applying IBC to reduce the vibrations for a six bladed, fully articulated rotor model are presented. It was found that - by using a linear, or in extension, a non-linear T-matrix approach - a good prediction for the achievable vibration reduction by means of single and mixed mode IBC can be achieved. This means that the numerical effort to calculate the optimal IBC input and to predict the possible reduction can be reduced by the proposed procedure. This is caused by the fact, that the numerical complexity of the T-matrix model is less than the underlying mod-

els as used in rotor dynamics simulation programs, e.g. S4.

For a considerable reduction of an overall vibration cost function the use of mixed mode IBC inputs is necessary. Using IBC mixed modes a significant reduction up to 80 percent was achieved. However, the frequencies and their number of which the mixed mode input consists vary over the flight envelope. This is a strong indicator for the necessity of a closed loop control scheme to reduce the vibrations over the whole flight envelope.

The ZFL is currently conducting flight trials with an IBC system on the CH-53G [17]. It is also involved in wind tunnel tests with an UH-60 rotor at the NASA Ames wind tunnel together with its partners NASA, Sikorsky Aircraft Corporation and Army/NASA Rotorcraft Division [16]. It is planned to validate the proposed method with the test data that are being collected during these two campaigns. In addition, the presented method may prove to become a suited design tool for future IBC systems in terms of predicting the required control authority and possible control performance.

Acknowledgement

The work presented in this paper has been partial funded by the aviation research program of the German Ministry of Economics and Technology under the contract number 20 H 9903.

References

[1] J.C. Houbolt, G.W. Brooks, *Differential Equations of Motion for Combined Flapwise Bending, Chordwise Bending, And Torsion of Twisted Nonuniform Rotor Blades*, NACA Technical Note 1346, 1957.

[2] R. Kube, B.G. van der Wall, K.-J. Schulz, W.R. Splettstoesser, *IBC Effects on BVI Noise and Vibrations – A Combined Numerical and Experimental Investigation*, 55th Annual Forum of the American Helicopter Society, Montreal, Canada, 1999.

[3] H. Honert, B.G. van der Wall, M. Fritzsche, G. Niesl, *Realtime BVI Noise Identification from Blade Pressure Data*, 24th European Rotorcraft Forum, Marseilles, France, 1998.

[4] P. Beaumier, J. Prieur, G. Rahier, P.Spiegel, A. Demargne, C. Tung, J.M. Gallman, Y.H. Yu, R. Kube, B.G. van der Wall, K.J. Schultz, W.R. Splettstoesser, T.F. Brooks, C.L. Burley, D.D. Boyd, *Effect of Higher Harmonic Control on Helicopter Rotor Blade-Vortex Interaction Noise: Prediction and Initial Validation*, 75th Fluid Dynamics Symposium (AGARD-CP-552), Berlin, Germany, 1994.

[5] D. Petot, G. Arnaud, R. Harrison, J. Stevens, D. Teves, B.G. van der Wall, C. Young, E. Szchnyi, *Stall Effects and Blade Torsion – an Evaluation of Predictive Tools*, 23rd European Rotorcraft Forum, Dresden, Germany, 1997.

[6] W.R Splettstoesser, B.G. van der Wall, B. Junker, K.-J. Schulz, P. Beaumier, Y Delrieux, P. Leconte, P. Crozier, *The ERATO Programme: Wind Tunnel Results and Proof of Design for an Acoustically Optimized Rotor*, 25th European Rotorcraft Forum, Rom, Italy, 1999.

[7] B.G. van der Wall, *An Analytical Model of Unsteady Profile Aerodynamics and its Application to a Rotor Simulation Program*, 15th European Rotorcraft Forum, Amsterdam, Netherlands, 1989.

[8] B.G. van der Wall, J.G. Leishman, *On the Influence of Time-Varying Flow Velocity on Unsteady Aerodynamics*, Journal of the American Helicopter Society, Vol. 39, No. 4, 1994.

[9] T.S. Beddoes, *A wake model for High Resolution Airloads,* US Army / AHS International Conference on Rotorcraft Basic Research, Research Triangle Park, NC, USA, 1985.

[10] B.G. van der Wall, *Der Einfluß aktiver Blattsteuerung auf die Wirbelbewegung im Nachlauf von Hubschrauberrotoren*, Dissertation Technische Universität Braunschweig, DLR-FB 99-34, Braunschweig, Germany, 1999.

[11] M. Müller, U.T.P. Arnold, D. Morbitzer, *On the Importance and Effectiveness of 2/rev IBC for Noice, Vibration and Pitch Link Load Reduction, 25th European Rotorcraft Forum, Rome, Italy, 1999.*

[12] W.L. Goffe, SIMANN: *A Global Optimization Algorithm using Simulated Annealing,* Studies in Nonlinear Dynamics and Econometrics, Vol. 1(3), pp. 169-175, 1996

[13] W-L- Goffe, G. Ferrier, J. Rogers, *Global Optimization of Statistical Functions with Simulated Annealing*, Journal of Econometrics, Vol. 60, No. 1/2, pp. 65-99, 1994.

[14] D. Morbitzer, U.T.P. Arnold, M. Müller, *Vibration and Noise Reduction through Individual Blade Control Experimental and Theoretical Results,* 24th European Rotorcraft Forum, Marseille, France, 1998.

[15] R. Kube, *Einfluss der Blattelastizität auf die höherharmonische Steuerung und Regelung eines gelenklosen Hubschrauberrotors*, DLR-FB-97-26, Braunschweig, 1997.

[16] S A Jacklin, A. Haber, G. de Simone, T.R. Norman, P. Shinoda, *Full-Scale Wind Tunnel Test of an Individual Blade Control System for a UH-60 Helicopter*, American Helicopter Society, 58th Annual Forum, Montréal, 2002.

[17] U.T.P. Arnold, G. Strecker, *Certification, Ground and Flight Testing of an Experimental IBC System for the CH-53G Helicopter,* American Helicopter Society, 58th Annual Forum, Montréal, 2002.

[18] M. Polychroniadis, M. Achache, *Higher Harmonic Control: Flight Tests of an Experimental System on SA 349 Research Gazelle*, American Helicopter Society 42nd Annual Forum, Washington, DC, 1986.

[19] F.R. Wood, R.W. Powers, J.H. Cline, C.E. Hammond, *On Developing and Flight Testing a Higher Harmonic Control System,* American Helicopter Society 39th Annual Forum, St. Lois, 1983.

[20] S.A. Jacklin, A. Blaas, D. Teves, R. Kube, *Reduction of Helicopter BVI Noise, Vibration and Power Consumption Through Individual Blade Control*, American Helicopter Society 51st Annual Forum, Fort Worth, 1995.

[21] W. Johnson, *CAMRAD/JA A Comprehensive Analytical Model of Rotorcraft Aerodynamics and Dynamics*, Theory and User Manual, 1988